A Comparative Study Between Eruptive X-class Flares Associated with Coronal Mass Ejections and Confined X-class Flares

Yuming Wang[1,2], and Jie Zhang[1]

ABSTRACT

Following the traditional naming of "eruptive flare" and "confined flares" but not implying a causal relationship between flare and coronal mass ejection (CME), we refer to the two kinds of large energetic phenomena occurring in the solar atmosphere as eruptive event and confined event, respectively: the former type refers to flares with associated CMEs, while the later type refers to flares without associated CMEs. We find that about 90% of X-class flares, the highest class in flare intensity size, are eruptive, but the rest 10% confined. To probe the question why the largest energy release in the solar corona could be either eruptive or confined, we have made a comparative study by carefully investigating 4 X-class events in each of the two types with a focus on the differences in their magnetic properties. Both sets of events are selected to have very similar intensity (X1.0 to X3.6) and duration (rise time less than 13 minutes and decaying time less than 9 minutes) in soft X-ray observations, in order to reduce the bias of flare size on CME occurrence. We find no difference in the total magnetic flux of the photospheric source regions for the two sets of events. However, we find that the occurrence of eruption (or confinement) is sensitive to the displacement of the location of the energy release, which is defined as the distance between the flare site and the flux-weighted magnetic center of the source active region. The displacement is 6 to 17 Mm for confined events, but is as large as 22 to 37 Mm for eruptive events, compared to the typical size of about 70 Mm for active regions studied. In other words, confined events occur closer to the magnetic center while the eruptive events tend to occur closer to the edge of active regions. Further, we have used potential-field source-surface model (PFSS) to infer the 3-D coronal magnetic field above source active regions. For each event, we calculate the coronal flux ratio of low corona ($< 1.1\ R_\odot$) to high corona ($\geq 1.1\ R_\odot$).

[1]Department of Computational and Data Sciences, College of Science, George Mason University, 4400 University Dr., MSN 6A2, Fairfax, VA 22030, USA, Email: ywangf@gmu.edu, jzhang7@gmu.edu

[2]School of Earth & Space Sci., Univ. of Sci. & Tech. of China, Hefei, Anhui 230026, China, Email: ymwang@ustc.edu.cn

We find that the confined events have a lower coronal flux ratio (< 5.7), while the eruptive events have a higher flux ratio(> 7.1). These results imply that a stronger overlying arcade field may prevent energy release in the low corona from being eruptive, resulting in flares without CMEs. A CME is more likely to occur if the overlying arcade field is weaker.

Subject headings: Sun: coronal mass ejections — Sun: flares — Magnetic Fields

1. Introduction

Coronal mass ejections (CMEs) and flares are known to be the two most energetic phenomena that occur in the atmosphere of the Sun, and have profound effects on the physical environment in the geo-space environment and human technological systems. In this paper, we intend to understand the physical origins of CMEs and flares by comparatively studying two different kinds of energetic phenomena, both of which have almost identical flares, but one is associated with CMEs and the other not. In the past when lacking direct CME observations, these two kinds of phenomena have been called as eruptive flares and confined flares, respectively (e.g., Svestka and Cliver 1992). An eruptive flare (also called a dynamic flare) is usually manifested as having two-ribbons and post-flare loops in Hα imaging observations and long duration (e.g., tens of minutes or hours) in soft X-ray, while a confined flare occurs in a compact region and last for only a short period (e.g., minutes). Following this convention but trying not to imply a causal relation between flare and CME, hereafter we refer the flare event associated with an observed CME as an "eruptive event", and the flare event not associated with a CME as a "confined event".

It has been suggested based on observations that CMEs and flares are the two different phenomena of the same energy release process in the corona (e.g., Harrison 1995; Zhang et al. 2001; Harrison 2003). They do not drive one another but are closely related. In particular, Zhang et al. (2001) and Zhang et al. (2004) showed that the fast acceleration of CMEs in the inner corona coincides very well in time with the rise phase (or energy release phase) of the corresponding soft X-ray flares, strongly implying that both phenomena are driven by the same process at the same time, possibly by magnetic field reconnections. However, this implication raises another important question of under what circumstances the energy release process in the corona leads to an eruption, and under what circumstances it remains to be confined during the process. An answer to this question shall shed the light on the origin of flares as well as CMEs.

The occurrence rate of eruptive events depends on the intensity and duration of flares.

A statistical study performed by Kahler et al. (1989) showed that the flares with longer duration tend to be eruptive, while more impulsive flares tend to be confined. By using the CME data from Solar Maximum Mission (SMM) and the flare data from GOES satellites during 1986 – 1987, Harrison (1995) found that the association ratio of flares with CMEs increases from about 7% to 100% as the flare class increases from B-class to X-class, and from about 6% to 50% as the duration of flares increases from about 1 to 6 hours. Andrews (2003) examined 229 M and X-class X-ray flares during 1996 – 1999, and found that the CME-association rate, or eruptive rate is 55% for M-class flares and 100% for X-class flares. With a much lager sample of 1301 X-ray flares, Yashiro et al. (2005) obtained a similar result that the eruptive rates of C, M, and X-class flares are $16-25\%$, $42-55\%$, and $90-92\%$, respectively. Yashiro et al. (2005) work showed that a flare is not necessarily associated with a CME even if it is as intense as an X-class flare. Such kind of confined but extremely energetic events were also reported by Feynman and Hundhausen (1994) and Green et al. (2002).

The studies mentioned above indicate the probability of CME occurrence for a given flare. On the other hand, there is also a probability of flare occurrence for a given CME. There are CMEs that may not be necessarily associated with any noticeable X-ray flares. Zhang et al. (2004) reported an extremely gradually accelerated slow CME without flare association, implying that the non-flare eruptive event tends to be slowly driven. By Combining the corona data from SMM and 6-hr soft X-ray data from GOES satellite, St. Cyr and Webb (1991) reported that about 48% frontside CMEs were associated with X-ray events near the solar minimum of solar cycle 21. Based on SOHO observations, Wang et al. (2002) studied 132 frontside halo CMEs, and found that the association rate of CMEs with X-ray flares greater than C-class increased from 55% at solar minimum to 80% near solar maximum. With 197 halo CMEs identified during 1997 – 2001, Zhou et al. (2003) concluded that 88% CMEs were associated with EUV brightenings.

Some attempts have been made to explain the confinement or the eruptiveness of solar energetic events in the context of the configuration of coronal magnetic field. Green et al. (2001) analyzed the 2000 September 30 confined event utilizing multi-wavelength data, and suggested that the event involve magnetic reconnection of two closed loops to form two newly closed loops without the opening of the involved magnetic structure. Nindos and Andrews (2004) made a statistical study of the role of magnetic helicity in eruption rate. They found that the coronal helicity of active regions producing confined events tends to be smaller than the coronal helicity of those producing eruptive events.

In this paper, we address the eruptive-confinement issue of solar energetic events with the approach of a comparative study. We focus on the most energetic confined events that

produce X-class soft X-ray flares but without CMEs. While the majority of X-class flares are eruptive, a small percentage (about 10%) of them are confined. The magnetic properties of these confined events shall be more outstanding than those less-energetic confined events. For making an effective comparison, we select eruptive events with X-ray properties, in terms of intensity and duration, very similar to those selected confined events. The differences on magnetic configuration between these two sets of events shall most likely reveal the true causes of eruption or confinement. How to select events and the basic properties of these events are described in section 2. Detailed comparative analyses of the two sets of events are given in section 3 and 4, which are on the properties of the photospheric magnetic field distribution and the extrapolated coronal magnetic field distribution, respectively. In section 5, we summarize the paper.

2. Selection of Events and Observations

2.1. Confined Events: X-class Flares without CMEs

From 1996 to 2004, there are 104 X-class soft X-ray flares reported by the NOAA (National Oceanic and Atmosphere Administration) Space Environment Center (SEC). Flares are observed by Geosynchronous Earth Observing Satellites (GOES), which record in high temporal resolution (every 3 seconds) the disk-integrated soft X-ray flux in two pass-bands: 1.0 – 8.0 Å and 0.5 – 4.0 Å, respectively. The flare catalog provides the peak intensity, beginning time, peak time, and ending time of flares. Based on peak intensity, flares are classified into five categories: A, B, C, M and X in the order of increasing strength. An X-class flare, in the strongest category, is defined by the peak flux in the 1.0 – 8.0 Å band exceeding 10^{-4} Wm^{-2}.

To find out whether a flare is associated with a CME or not, we make use of both the CME observations by Large Angle and Spectrometric Coronagraph (LASCO, Brueckner et al. 1995) and coronal disk observations by Extreme Ultraviolet Imaging Telescope (EIT, Delaboudiniere et al. 1995); both instruments are on-board the Solar and Heliospheric Observatory (SOHO) spacecraft. The search process started with the CME catalog[1] (Yashiro et al. 2004) for an initial quick look. A flare becomes a candidate of confined type if there is no any CME whose extrapolated onset time is within the 60-minute time window centered at the fare onset time. The onset time of a CME is calculated by linearly extrapolating the height-time measurement in the outer corona back to the surface of the Sun, which shall give the first-order

[1]the NRL-GSFC-CUA CME catalog at http://cdaw.gsfc.nasa.gov/CME_list/

approximation of the true onset time of CME. Further, we visually examine the sequence of the LASCO and EIT images around the flare time to verify that indeed there is no CME associated with the flare studied. One common property of these confined events is the lack of EUV dimming in EIT images, even though they show strong compact brightenings in EIT images. Following the compact brightening, there is no corresponding CME feature appearing in subsequent LASCO images. This scenario is in sharp contrast to that of an eruptive event, in which an EIT dimming accompanies the brightening, and within a few frames, a distinct CME feature appears in appropriate position angle in LASCO images. After applying this process on all X-class flares, we find 11 events are confined; they are listed in Table 1. We notice that event 7 to 11 occurred within three days between July 15 - 17, 2004, and they all originated from the same solar active region (NOAA AR10649).

Among the 11 confined X-class flares from 1996 to 2004, the first four events have been reported earlier by Yashiro et al. (2005).The third one has also been reported and studied by Green et al. (2002). During 1996 – 2004, there are in total 104 X-class flares. Thus the percentage of confined X-class flares is about 10%. As shown in Table 1, all these confined flares are impulsive. Their rise time does not exceed 13 minutes except for event 8 (23 minutes). The decay time does not exceed 10 minutes for all the 11 events. The rise and decay times are derived from the begin, maximum and end times of flares, which are defined and compiled by NOAA/SEC [2]. The peak intensity of all these events was less than X2.0 level except for event 10 (X3.6). Any event stronger than X3.6 is found always associated with a CME.

Out of the 11 confined events, we are able to select 4 of them suitable for further in-depth analysis. These events are numbered as 4, 5, 6 and 11, respectively. They are suitable because (1) the flare is isolated, which means that there is no other flare immediately preceding and following that flare, and (2) there is no other coronal dimming or CME eruption in the vicinity of the flare region within a certain period. Events 1 and 3 are not selected, because they mixed up with a flare-CME pair from the same source regions. In the presence of an eruptive flare immediately preceding or following a confined event, we are not certain how well the confined event is related with the earlier or later eruptive one. In order to make our analysis as "clean" as possible, such events are discarded. Event 2 is also excluded because its source region is right behind the western limb and hence no timely magnetogram data is available. Events 7 through 11 were all from the same active region. By over-plotting EIT images showing flare locations on the MDI magnetogram images, we find that these flares essentially occurred at the same location within the active region. Thus we choose only

[2]http://www.sec.noaa.gov/ftpdir/indices/events/README

the last event representing all the five events. The four confined events selected for further analysis are labelled by C_1 through C_4 in the second column of Table 1.

2.2. Eruptive Events: X-class Flares with CMEs

For making the comparative study with the 4 confined events mentioned above, a set of four eruptive X-class flares are selected. These eruptive flares are chosen to have similar properties in X-rays as those confined events:(1) their rise time and decay time are less than 13 minutes, (2) their intensities are between X1.0 to X2.0. Further, their locations are within 60° from solar central meridian in longitude in order to reduce the projection effect in magnetograms. These flares, which are relatively impulsive, are indeed associated with CMEs, as shown in LASCO images. The four events are also listed in Table 1 labelled as E_1 through E_4, respectively.

An overview of the two sets of events is given in Figure 1. The upper panels show the four confined events and the lower panels show the four eruptive events. For each event we show the GOES soft X-ray flux profile (all in a 2-hour interval), running-difference EIT image and running-difference LASCO image in the top, middle and low panels, respectively. Apparently, the temporal profiles of GOES soft X-ray fluxes exhibit no noticeable difference between the two sets of events, due to the constraint in our selection of events. Moreover, as seen in the EIT images, the two sets of events are all associated with compact coronal brightening indicating the occurrence of flares. However, for eruptive flares, the accompanying CMEs are clearly seen in those LASCO images. In contrast, there is no apparent brightening CME feature seen in LASCO images for those confined events (only one image is shown here to represent the observed sequence of images, which all indicate a non-disturbed corona). For eruptive events, the speeds and angular widths of CMEs are also listed in the Table 1.

3. Magnetic Properties in the Photosphere

3.1. Flare Location and Active Region Morphology

To explore what physical factors lead the two similar sets of flares, all strong and impulsive, to have difference in CME production, we first study the magnetic properties of their surface source regions. SOHO/MDI provides the observations of photospheric magnetic field (the component along the line of sight) every 96 minutes. The spatial resolution of MDI magnetograms is about 4 arcsec with a plate scale of 2 arcsec per pixel, at which detailed magnetic features across the source active regions are reasonably resolved. To reduce the

projection effect of line-of-sight magnetic field, we have only chosen the events within 60° from solar central meridian.

For each event, we determine the location of the flare seen in EIT relative to the magnetic features seen in MDI. We first align the MDI image with the corresponding EIT image. The difference in the timing between MDI and EIT images have been taken into account. Figure 2 illustrates the alignment for the 2001 June 23 event. The soft X-ray flare began at 04:02 UT and peaked at 04:09 UT. In EIT 195 Å image showing the flare was taken at 04:11 UT. The nearest full disk MDI image prior to the flare was taken at 03:11 UT. The MDI magnetogram is rotated to fit the EIT time, and then superimposed in contours onto the EIT image. In the right panel of Figure 2, we display the aligned images; only the region of interest is shown. Using this method, we are able to determine the location of flares, which is just above the neutral lines seen in the magnetogram.

In Figure 3 and 4, we show the magnetogram images for the four confined events and the four eruptive events, respectively. The flare sites, or bright patches seen in EIT, are marked by red asterisks in the images. The magnetogram images have been re-mapped onto the Carrington coordinate, which reduces the spherical projection effect of the image area. The x-axis is Carrington longitude in units of degree, and the y-axis is the sine of latitude. The area of the images shown in Figure 3 and 4 are all $30^\circ \times 30^\circ$ squares, which usually cover the entire active regions producing the CMEs/flares of interest. To highlight the magnetic features, the displayed images have been segmented into three different levels: strong positive magnetic field (≥ 50 Gauss) indicated by white color, strong negative magnetic field (≤ -50 Gauss) indicated by black color, and weak field (from -50 to 50 Gauss) indicated by gray color. Note that the noise level of a MDI magnetogram image is typically at about 10 Gauss. As shown in the figures, an active region is naturally segmented into many individual pieces. Those pieces with magnetic flux larger than 10^{13} wb are labelled by a letter with a number in the neighbouring bracket indicating the magnetic flux in units of 10^{13} wb.

3.2. Results

We find that there is no apparent difference in term of total magnetic flux of the source region between the confined events and eruptive events. The total magnetic flux, combining both positive and negative flux, are listed in Table 2. The total flux for confined events varies from about 5 to 36×10^{13} wb, while for eruptive events it varies from about 11 to 24×10^{13} wb.

However, there is a noticeable pattern that the confined flares all originated in a location

relatively closer to the center of the host active region. Figure 3a shows the confined event of 2001 June 23. There are three relatively large magnetic pieces labelled by 'A', 'B' and 'C'. The flare site is surrounded by the pieces 'A' and 'B'. Figure 3b shows the 2003 August 9 confined event. The flare location is associated with three small negative patches (marked by the red asterisks) embedded in a large positive piece 'A'. Figure 3c shows the 2004 February 26 confined event. The flare occurred just above the neutral line between thye large positive piece 'A' and the large negative piece 'B'. Figure 3d shows the 2004 July 17 confined event. The flare was located in a complex active region with a large number of sunspots. It occurred right at the boundary between pieces 'C' and 'F'. From the view of the entire active region, pieces 'C' and 'F' were further enclosed by two much larger and stronger pieces 'A' and 'D' whose fluxes were about 10 times larger.

For those eruptive flares, on the other hand, the flare sites were all relatively further from the center of the magnetic flux distribution. In other words, they were closer to the edge of hosting active regions. Figure 4a shows the 1998 May 2 event. The strongest pair of magnetic pieces are 'A' and 'D', but the eruptive flare occurred at the neutral line between pieces 'D' and 'C', which was the smallest amongst the 4 labelled pieces in the active region. Figure 4b shows the 2000 March 2 event. Similarly, the strongest pair of pieces were 'A' and 'C', but the flare was from the neutral line between pieces 'C' and 'B', which was the smallest labelled piece. Figure 4c shows the 2000 November 24 event. The flare occurred at the outer edge of the strongest piece 'A', which was neighbored by a very small region with negative flux. Figure 4d shows the 2004 October 30 event. The flare site was also close to the edge of the entire active region.

To quantify this observation of different displacements of flare locations, we here introduce a flare displacement parameter, which is defined by the surface distance between the flare site and the weighted center of the magnetic flux distribution of the host active region, or center of magnetic flux (COM) for short. The COM might be the place that has the most overlying magnetic flux. The COM is calculated based on the re-mapped $30^\circ \times 30^\circ$ MDI images (without segmentation). It is a point, across which any line can split the magnetogram into two flux-balanced halves, and can be formulated as $x_c = \frac{\sum_i F_i * x_i}{\sum_i F_i}$ and $y_c = \frac{\sum_i F_i * y_i}{\sum_i F_i}$. The COM of these events have been marked by the diamonds in Figure 3 and 4. With known COM, it is easy to derive the displacement parameter, which is listed in Table 2. Consistent with the earlier discussions, it is found that the displacement parameters for the four confined events are all smaller than 17 Mm, while for the four eruptive events, they are all larger than 22 Mm.

We now consider possible errors in calculating the displacement parameter. The error main arises from the uncertainty in the recorded weak magnetic field around the active

regions. However, in the selected region of study that is $30^\circ \times 30^\circ$ across, the highlighted white and black pieces contain about 99% of the total magnetic flux in the region. Therefore the uncertainty of the flux is expected to be at the order of 1%. Considering the formula of the coordinates of COM given in the last paragraph and assuming a typical scale of 100 Mm, the error of the calculated distance is about 1 Mm. Further, considering the spatial resolution of MDI of $\sim$ 1 Mm (varing from $\sim$ 0.7 Mm at central meridian to $\sim$ 1.4 Mm at longitude of $\pm 60^\circ$), the overall uncertainty should be about ± 2 Mm. With these consideration, the displacement parameters and their uncertainties are plotted in Figure 7. The confined events are indicated by diamonds, and the eruptive events are indicated by asterisks. The vertical dashed line, which corresponds to a displacement of about 19.5 Mm, effectively separates the two sets of events.

4. Magnetic Properties in the Corona

4.1. Method

Having studied the magnetic field distributions in the photosphere, we further investigate into magnetic field distributions in the 3-D corona. The magnetic field configuration in the corona shall ultimately determine the eruption/confinement since the energy releases occurs in the corona. There is so far no direct observations of coronal magnetic fields. We have to utilize certain models to calculate the coronal magnetic field based on observed photospheric boundary. In this paper, we apply the commonly used potential-field source-surface (PFSS) model (e.g., Schatten et al. 1969; Hoeksema et al. 1982). The PFSS model is thought to be a useful first-order approximation to the global magnetic field of the solar corona. Nevertheless, we realize that the current-carrying core fields, which are low-lying and near the magnetic neutral line, are far from the potential field approximation; these core fields are likely to be the driving source of any energy release in the corona. Therefore, the usage of PFSS model in this study is limited to calculate the total flux of the overlying large scale coronal field, which is believed to be closer to a potential approximation. These overlying fields are thought to constrain the low-lying field from eruption.

A modified MDI magnetic field synoptic chart is used as input to our PFSS model. The high-resolution MDI magnetic field synoptic chart[3] is created by interpolating data to disk-center resolution, resulting in a 3600×1080 pixel map. The X and Y axis are linear in Carrington longitude (0.1° intervals) and sine latitude, respectively. This high resolution

[3]http://soi.stanford.edu/magnetic/index6.html

is useful in creating detailed coronal magnetic field above the source regions of interest. Since an MDI synoptic chart is created from the magnetogram images over a $\sim$ 27-day solar rotation, the synoptic chart does not exactly represent the photospheric magnetic field in the region of interest at the flare/CME time. The details of the source region may be different because of the evolution of photospheric magnetic field. To mitigate this problem, we use the MDI daily magnetogram to update the original MDI synoptic chart. The process is to re-map the snapshot magnetogram image prior to the flare occurrence to the Carrington grid, and then slice out the region of interest, 30° in longitude and 60° in latitude. This sliced region, to replace the corresponding portion in the original synoptic chart.

Since a PFSS model makes use of the spheric harmonic series expansion, we realize that a high-resolution data requires a high order expansion in order to have a consistent result. We calculate the spheric harmonic coefficients to as high as 225 order for the input 3600×1080 boundary image. We find that, at this order, we can get the best match between the calculated photospheric magnetic field and the input synoptic chart. The mean value of the difference between them is less than 0.5 Gauss, and the standard deviation is generally $\lesssim$ 15 Gauss for solar minimum and $\lesssim$ 25 Gauss for solar maximum, which are comparable to the noise level of MDI magnetograms. That means, we can effectively reproduce the observed photospheric magnetic field with the 225-order PFSS model. With spheric harmonic coefficients known, it is relatively straightforward to calculate the magnetic field in the 3-D volume of the corona.

4.2. Results

Figure 5 and 6 show the extrapolated coronal magnetic field lines for one confined event (2004 July 17) and one eruptive event (2004 October 30), respectively. In each figure, the left panel shows field lines viewed from top, and the right panel shows field lines viewed from the side by rotating the left panel view of 60 degrees into the paper. The green-yellow colors denote the closed field lines, with green indicating the loop part of outward magnetic field (positive magnetic polarity at the footpoints) and yellow the inward (negative magnetic polarity at the footpoints), and the blue color indicates the open field lines. The two examples show that the location of the confined flare, which is near the center of the active region, is covered by a large tuft of overlying magnetic loop arcades, while the location of the eruptive flare, which is near the edge of the active region, has relatively few directly overlying loop arcade. In particular, for the eruptive event, the nearby positive and negative magnetic field lines seem to connect divergently with other regions, instead of forming a loop arcade of its own.

To quantify the strength of the overlying field, we calculate the total magnetic flux cross the plane with the x direction extending along the neutral line and the y direction vertically along the radial direction. The thick blue lines on the photospheric surface in Figure 3 and 4 indicate the neutral lines used in the calculation. The length of the neutral lines is determined as it encompasses the major part of the eruption region. The overlying magnetic field flux then is normalized to the length of the neutral line. Thus obtained normalized overlying magnetic flux is a better quantity to be used for comparison between different events, because this parameter is not sensitive to the exact length of the neutral lines selected, which may vary significantly from event to event.

Such calculated magnetic fluxes for the 8 events are listed in Table 3. In calculating the flux, we do not consider that the crossing direction of the field lines over the neutral line is from one side to the other or opposite. The relative uncertainty of the calculated magnetic flux can be estimated as σ_B/B_0 where σ_B is the uncertainty of calculated magnetic field strength in the corona and B_0 is the magnetic field strength in the active regions at photosphere. Considering σ_B is about 15 to 25 Gauss, the standard deviation mentioned before, and B_0 is usually hundreds of Gauss, we infer that the uncertainty of overlying magnetic flux is about 10%. The estimate should be true in case that the coronal magnetic field is correctly obtained by our extrapolation method. If the extrapolated field largely deviates from the realistic status, the uncertainty may probably be slightly different.

The total overlying flux, F_{total}, in the height range from 1.0 to 1.5 $R_\odot$, is given in the third column. It seems that there is no systematic difference between the confined events and eruptive events. The value for the confined events varies from 0.40 to 1.27 $\times 10^{10}$ wb/Mm, and that for the eruptive events from 0.73 to 1.34 $\times 10^{10}$ wb/Mm.

We further calculate the flux in two different height ranges, the lower flux from 1.0 to 1.1 $R_\odot$ and the higher flux from 1.1 to 1.5 $R_\odot$. A common accepted scenario is that the lower flux shall correspond to the inner sheared core field (or fully-fledged flux rope if filament present) that tends to move out, while the outer flux is the large scale overlying arcade that tends to constrain the inner flux from eruption. Note that the chosen of 1.1 $R_\odot$, which corresponds to a height of about 70 Mm above the surface, is rather arbitrary. However, slightly changing this number will not affect any overall results that will be reached. The magnetic flux in the low corona, F_{low}, and in the high corona, F_{high}, are listed in the fourth and fifth columns of Table 3, respectively.

There is a trend that the low-corona flux for the eruptive events is generally larger than that for the confined events. Three out of the four eruptive events have their low-corona overlying flux more than 1.0 $\times 10^{10}$ wb/Mm, while three out of the four confined events have the flux less than 1.0 $\times 10^{10}$ wb/Mm. On the other hand, the high-corona flux for the

eruptive events seems smaller than that for the confined events. Three confined events have their high-corona flux more than 0.15 $\times 10^{10}$ wb/Mm, while all four eruptive events have the flux less than 0.15 $\times 10^{10}$ wb/Mm.

We further calculate the flux ratio parameter, which is defined as $R = F_{low}/F_{high}$. This quantity is independent of the normalization. It may serve as an index of how weak the constraint on the inner eruptive field is. Interestingly, the flux ratios for the two sets of events fall into two distinct groups. For the confined events, R varies from 1.59 to 5.68, while for the eruptive events, the value of R is larger, from 7.11 to 10.17. The value of 6.5 may be used as a boundary separating the two sets of events. This value probably implies a threshold for confinement or eruptiveness. This is to say, if the flux ratio is less than 6.5, a flare is likely to be confined, otherwise eruptive. The higher the ratio, the higher the possibility of a coronal energy release being eruptive.

5. Summary and Discussions

In summary, among the 104 X-class flares occurred during 1996 – 2004, we found a total of 11 ($\sim 10\%$) are confined flares without associated CMEs, and all the others ($\sim 90\%$) are eruptive flares associated with CMEs. Four suitable confined flares are selected to make a comparative study with four eruptive flares, which are similar in X-ray intensity and duration as those confined events. We have carefully studied the magnetic properties of these events both in the photosphere and in the corona. The following results are obtained:

(1) In the photosphere, we can not find a difference of the total magnetic fluxes in the surface source regions between the two sets of events. However, there is an apparent difference in the displacement parameter, which is defined as the surface distance between the flare site and the center of magnetic flux distribution. For the confined events, the displacement is from 6 to 17 Mm, while for those eruptive events it is from 22 to 37 Mm. This result implies that the energy release occurring in the center of an active region is more difficult to have a complete open eruption, resulting in a flare without CME. On the other hand, the energy release occurring away from the magnetic center has a higher probability to have an eruption, resulting in both flares and CMEs. Whether an eruption could occur or not may be strongly constrained by the overlying large scale coronal magnetic field. The overlying coronal magnetic field shall be strongest and also longest along the vertical direction over the center of an active region. On the other hand, the overlying constraining field shall be weaker if the source is away from the center. This scenario is further supported by our study of coronal magnetic field.

(2) Calculation of coronal magnetic field shows that the flux ratio of the magnetic flux in the low corona to that in the high corona is systematically larger for the eruptive events than that for the confined events. The magnetic flux ratio for the confined events varies from 1.6 to 5.7, while the ratio for the eruptive events from 7.1 to 10.2. However, there is no evident difference between the two sets of events in the total magnetic flux straddling over neutral lines, and there is only a weak trend indicating a systematic difference in the low- and high-corona magnetic fluxes. This low-to-high corona magnetic flux ratio serves as a proxy of the strength of the inner core magnetic field, which may play an erupting role, relative to the strength of the overlying large scale coronal magnetic field, which may play a constraining role to prevent eruption. The lower this ratio, the more difficult the energy release in the low corona can be eruptive.

There is variety of theoretical models on the initiation mechanism of CMEs and the energy release of flares (e.g., Sturrock 1989; Chen 1989; van Ballegooijen and Martens 1989; Forbes and Isenberg 1991; Moore and Roumeliotis 1992; Low and Smith 1993; Mikic and Linker 1994; Antiochos et al. 1999; Lin and Forbes 2000). These models differ in pre-eruption magnetic configurations, trigger processes, or where magnetic reconnection occurs. Nevertheless, in almost all these models, the magnetic configuration involves two magnetic regimes, one is the core field in the inner corona close to the neutral line, the other is the large scale overlying field or background field. The core field is treated as highly sheared or as a fully-fledged flux rope; in either case, the core field stores free energy for release. On the other hand, the overlying field is regarded as potential and considered to be main constraining force to prevent the underlying core field from eruption or escaping. Torok and Kliem (2005) and Kliem and Torok (2006) recently pointed out that the decrease of the overlying field with height is a main factor in deciding whether the kink-instability (in their twist flux rope model) leads to a confined event or a CME. On the other hand, Mandrini et al. (2005) reported the smallest CME event ever observed by 2005, in which the CME originated from the smallest source region, a tiny dipole, and developed into the smallest magnetic cloud. They suggested that the ejections of tiny flux ropes are possible. Therefore, it is reasonable to argue that, whether an energy release in the corona is eruptive or confined, is sensitive to the balance between the inner core field and the outer overlying field. Our observational results seem to be consistent with this scenario.

This study is only a preliminary step to investigate the confinement and/or eruptiveness of solar flares, or coronal energy releases in general. However, it demonstrates that the distribution of magnetic field both in the photosphere and in the corona may effectively provide the clue of the possible nature of an energetic event: whether a flare, a CME or both. To further evaluate the effectiveness of this methodology, a more robust study involving more events is needed.

We acknowledge the use of the solar data from the LASCO, EIT and MDI instruments on board SOHO spacecraft. The SOHO/LASCO data used here are produced by a consortium of the Naval Research Laboratory (USA), Max-Planck-Institut fuer Aeronomie (Germany), Laboratoire d'Astronomie (France), and the University of Birmingham (UK). SOHO is a project of international cooperation between ESA and NASA. We also acknowledge the use of CME catalog generated and maintained at the CDAW Data Center by NASA and The Catholic University of America in cooperation with the Naval Research Laboratory, and the solar event reports compiled by the Space Environment Center of NOAA. We thank the useful discussion with X. P. Zhao at Stanford University, who provides the procedure of PFSS model. This work is supported by NSF SHINE grant ATM-0454612 and NASA grant NNG05GG19G. Y. Wang is also supported by the grants from NSF of China (40525014) and MSTC (2006CB806304), and J. Zhang is also supported by NASA grants NNG04GN36G.

REFERENCES

Andrews, M. D.: 2003, A search for CMEs associated with big flares, *Sol. Phys.* **218**, 261–279.

Antiochos, S. K., DeVore, C. R. and Klimchuk, J. A.: 1999, A model for solar coronal mass ejections, *Astrophys. J.* **510**, 485–493.

Brueckner, G. E., Howard, R. A., Koomen, M. J., Korendyke, C. M., Michels, D. J., Moses, J. D., Socker, D. G., Dere, K. P., Lamy, P. L., Llebaria, A., Bout, M. V., Schwenn, R., Simnett, G. M., Bedford, D. K. and Eyles, C. J.: 1995, The large angle spectroscopic coronagraph (LASCO), *Sol. Phys.* **162**, 357–402.

Chen, J.: 1989, Effects of toroidal forces in current loops embedded in a background plasma, *Astrophys. J.* **338**, 453–470.

Delaboudiniere, J.-P., Artzner, G. E., Brunaud, J. and et al.: 1995, EIT: Extreme-ultraviolet imaging telescope for the SOHO mission, *Sol. Phys.* **162**, 291–312.

Feynman, J. and Hundhausen, A. J.: 1994, Coronal mass ejections and major solar flares: The great active center of march 1989, *J. Geophys. Res.* **99(A5)**, 8451–8464.

Forbes, T. G. and Isenberg, P. A.: 1991, A catastrophe mechanism for coronal mass ejections, *Astrophys. J.* **373**, 294–307.

Green, L. M., Harra, L. K., Matthews, S. A. and Culhane, J. L.: 2001, Coronal mass ejections and their association to active region flaring, *Sol. Phys.* **200**, 189–202.

Green, L. M., Matthews, S. A., van Driel-Gesztelyi, L., Harra, L. K. and Culhane, J. L.: 2002, Multi-wavelength observations of an x-class flare without a coronal mass ejection, *Sol. Phys.* **205**, 325–339.

Harrison, R. A.: 1995, The nature of solar flares associated with coronal mass ejection, *Astron. & Astrophys.* **304**, 585–594.

Harrison, R. A.: 2003, Soho observations relating to the association between flares and coronal mass ejections, *Adv. Space Res.* **32(12)**, 2425–2437.

Hoeksema, J. T., Wilcox, J. M. and Scherrer, P. H.: 1982, Structure of the heliospheric current sheet in the early portion of sunspot cycle 21, *J. Geophys. Res.* **87**, 10331–10338.

Kahler, S. W., Sheeley, Jr., N. R. and Liggett, M.: 1989, Coronal mass ejections and associated X-ray flare durations, *Astrophys. J.* **344**, 1026–1033.

Kliem, B., and Torok, T.: 2006, Torus Instability, *Phys. Rev. Lett.* **96**, 255002.

Lin, J. and Forbes, T. G.: 2000, Effects of reconnection on the coronal mass ejection process, *J. Geophys. Res.* **105(A2)**, 2375–2392.

Low, B. C. and Smith, D. F.: 1993, The free energies of partially open coronal magnetic fields, *Astrophys. J.* **410**, 412–425.

Mandrini, C. H., Pohjolainen, S., Dasso, S., Green, L. M., Demoulin, P., van Driel-Gesztelyi, L., Copperwheat, C. and Foley, C.: 2005, Interplanetary flux rope ejected from an X-ray bright point: The smallest magnetic cloud source-region ever observed, *Astron. & Astrophys.* **434**, 725–740.

Mikic, Z. and Linker, J. A.: 1994, Disruption of coronal magnetic field arcades, *Astrophys. J.* **430**, 898–912.

Moore, R. L. and Roumeliotis, G.: 1992, Triggering of eruptive flares - destabilization of the preflare magnetic field configuration, *in* Z. Svestka, B. V. Jackson and M. Machado (eds), *Eruptive Solar Flares*, Proceedings of IAU Colloquium No. 113, Springer-Verlag, New York, pp. 107–121.

Nindos, A. and Andrews, M. D.: 2004, The association of big flares and coronal mass ejections: What is the role of magnetic helicity?, *Astrophys. J.* **616**, L175–L178.

Schatten, K. H., Wilcox, J. M. and Ness, N. F.: 1969, A model of interplanetary and coronal magnetic fields, *Sol. Phys.* **6**, 442–455.

St. Cyr, O. C. and Webb, D. F.: 1991, Activity associated with coronal mass ejections at solar minimum - SMM observations from 1984-1986, *Sol. Phys.* **136**, 379–394.

Sturrock, P. A.: 1989, The role of eruption in solar flares, *Sol. Phys.* **121**, 387–397.

Svestka, Z. and Cliver, E. W.: 1992, History and basic characteristics of eruptive flares, *in* Z. Svestka, B. V. Jackson and M. E. Machado (eds), *Eruptive Solar Flares*, Proceedings of IAU Colloquium No. 113, Springer-Verlag, New York, pp. 1–11.

Torok, T. and Kliem, B.: 2005, Confined and ejective eruptions of kink-unstable flux ropes, *Astrophys. J.* **630**, L97–L100.

van Ballegooijen, A. A. and Martens, P. C. H.: 1989, Formation and eruption of solar prominences, *Astrophys. J.* **343**, 971–984.

Wang, Y. M., Ye, P. Z., Wang, S., Zhou, G. P. and Wang, J. X.: 2002, A statistical study on the geoeffectiveness of earth-directed coronal mass ejections from March 1997 to December 2000, *J. Geophys. Res.* **107(A11)**, 1340, doi:10.1029/2002JA009244.

Yashiro, S., Gopalswamy, N., Akiyama, S., Michalek, G. and Howard, R. A.: 2005, Visibility of coronal mass ejections as a function of flare location and intensity, *J. Geophys. Res.* **110(A12)**, A12S05.

Yashiro, S., Gopalswamy, N., Michalek, G., St. Cyr, O. C., Plunkett, S. P., Rich, N. B. and Howard, R. A.: 2004, A catalog of white light coronal mass ejections observed by the soho spacecraft, *J. Geophys. Res.* **109(A7)**, A07105.

Zhang, J., Dere, K. P., Howard, R. A., Kundu, M. R. and White, S. M.: 2001, On the temporal relationship between coronal mass ejections and flares, *Astrophys. J.* **559**, 452–462.

Zhang, J., Dere, K. P., Howard, R. A. and Vourlidas, A.: 2004, A study of the kinematic evolution of coronal mass ejections, *Astrophys. J.* **604**, 420–432.

Zhou, G., Wang, J. and Cao, Z.: 2003, Correlation between halo coronal mass ejections and solar surface activity, *Astron. & Astrophys.* **397**, 1057.

Table 1: List of Confined X-class Flares from 1996 to 2004 and Selected Eruptive Flares

#	Label	Date	Begin UT	T_R^a min	T_D^b min	Class	Location	NOAA AR	CME[c] V(km/s)/Width	Comment
					Confined Flares					
1		2000/06/06	13:30	9.0	7.0	X1.1	N20E18	9026	-	Contained by a preceding and a following M-class flares (Y)
2		2000/09/30	23:13	8.0	7.0	X1.2	N07W91	9169	-	Limb event (G, Y)
3		2001/04/02	10:04	10.0	6.0	X1.4	N17W60	9393	-	Contained by a preceding eruptive flare (Y)
4	C_1	2001/06/23	04:02	6.0	3.0	X1.2	N10E23	9511	-	(Y)
5	C_2	2003/06/09	21:31	8.0	4.0	X1.7	N12W33	10374	-	
6	C_3	2004/02/26	01:50	13.0	7.0	X1.1	N14W14	10564	-	
7		2004/07/15	18:15	9.0	4.0	X1.6	S11E45	10649	-	
8		2004/07/16	01:43	23.0	6.0	X1.3	S11E41	10649	-	
9		2004/07/16	10:32	9.0	5.0	X1.1	S10E36	10649	-	
10		2004/07/16	13:49	6.0	6.0	X3.6	S10E35	10649	-	
11	C_4	2004/07/17	07:51	6.0	2.0	X1.0	S11E24	10649	-	Event 7–11 all from the same AR
					Eruptive Flares					
1	E_1	1998/05/02	13:31	11.0	9.0	X1.1	S15W15	8210	936/halo	
2	E_2	2000/03/02	08:20	8.0	3.0	X1.1	S18W54	8882	776/62°	
3	E_3	2000/11/24	04:55	7.0	6.0	X2.0	N19W05	9236	1289/halo	
4	E_4	2004/10/30	11:38	8.0	4.0	X1.2	N13W25	10691	427/halo	

[a] Rise time of flares.

[b] Decay time of flares.

[c] Apparent speed and angular width of CMEs. Adopted from the online GSFC-NRL-CUA CME catalog. G and Y in comment column mean that the corresponding events have been reported by Green et al. (2002) and Yashiro et al. (2005), respectively.

Table 2: Magnetic Properties of the Source Active Regions of the Confined and Eruptive Flares

Event	Date	Flux[a]	Distance[b]
		10^{13} wb	Mm
	Confined Flares		
C_1	2001/06/23	5	6
C_2	2003/06/09	36	17
C_3	2004/02/26	23	8
C_4	2004/07/17	34	10
	Eruptive Flares		
E_1	1998/05/02	17	22
E_2	2000/03/02	24	33
E_3	2000/11/24	18	37
E_4	2004/10/30	11	29

[a] Total magnetic flux in active regions measured in MDI magnetogram.

[b] Surface distance between the flare site and the COM of the associated active region.

Table 3: Magnetic flux per unit length overlying the neutral lines

Event	Date	F_{total}	F_{low}	F_{high}	Ratio= $\frac{F_{low}}{F_{high}}$
		10^{10} wb/Mm	10^{10} wb/Mm	10^{10} wb/Mm	
			Confined Flares		
C_1	2001/06/23	0.40	0.34	0.06	5.67
C_2	2003/06/09	0.83	0.61	0.22	2.77
C_3	2004/02/26	1.27	1.08	0.19	5.68
C_4	2004/07/17	1.19	0.73	0.46	1.59
			Eruptive Flares		
E_1	1998/05/02	1.34	1.22	0.12	10.17
E_2	2000/03/02	1.17	1.06	0.11	9.64
E_3	2000/11/24	1.14	1.03	0.11	9.36
E_4	2004/10/30	0.73	0.64	0.09	7.11

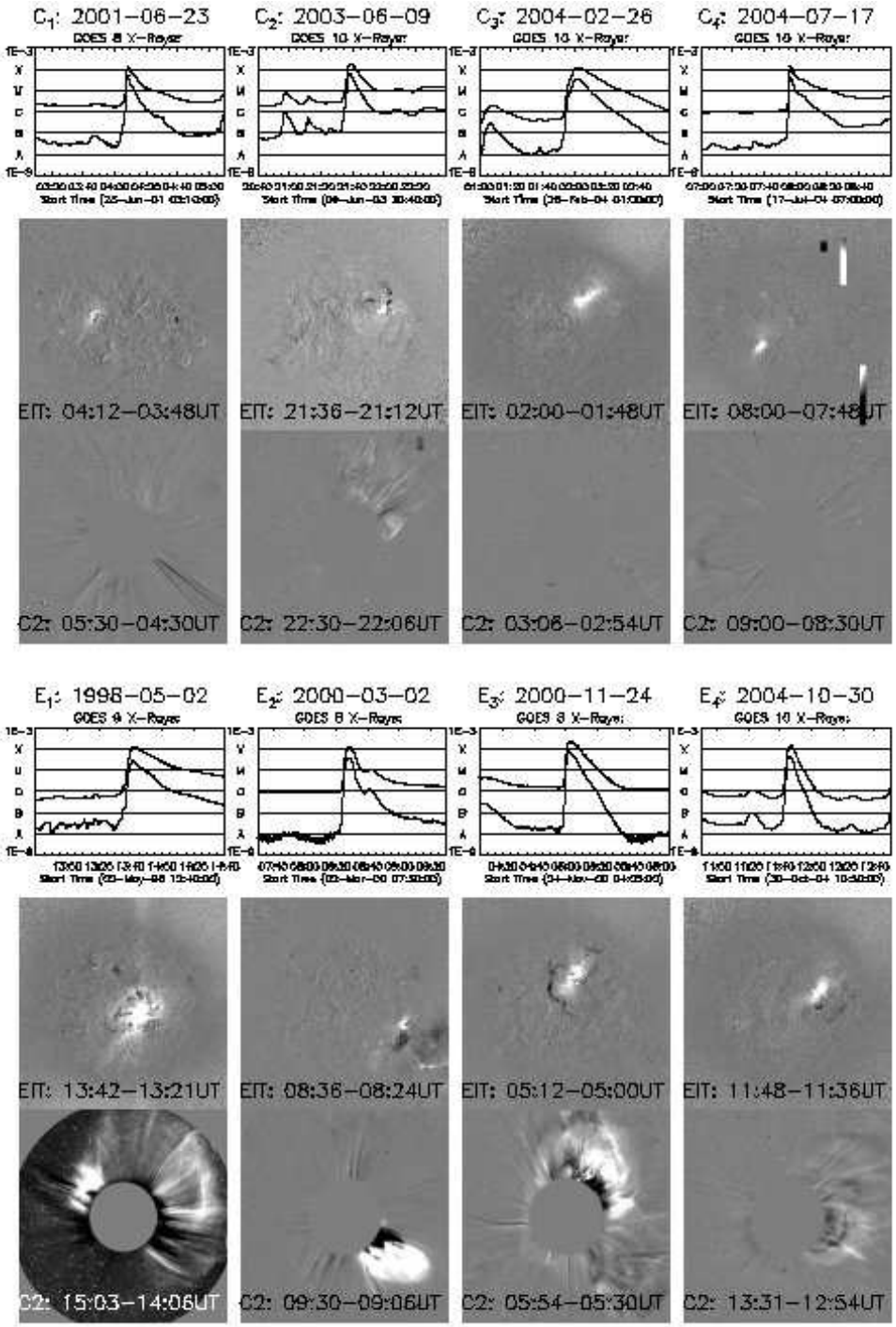

Fig. 1.— An overview of the four confined (C_1-C_4, upper panels) and four eruptive (E_1-E_2, lower panels) flares. For each events, we display its GOES X-ray flux profile (spanning 2 hours), running-difference images of EIT 195Å and LASCO/C2 in the three sub-panels from top to bottom.

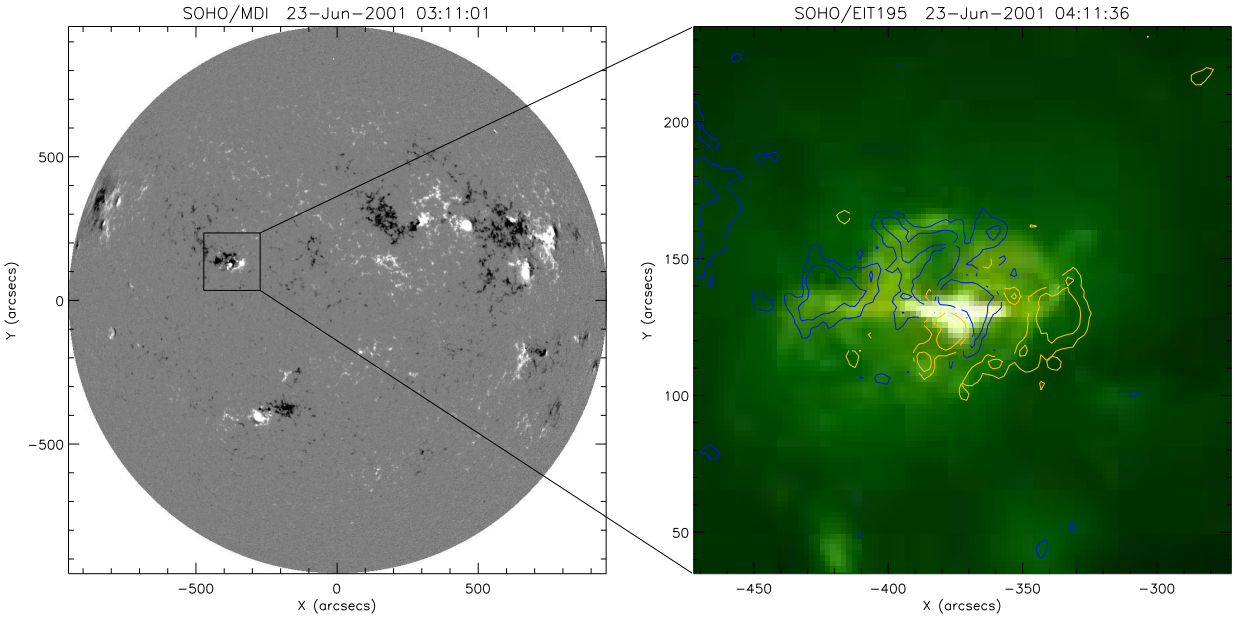

Fig. 2.— An example showing flare and its source region. The left image is a full disk MDI magnetogram taken before the flare onset. The right image shows the EIT image in green-white false colors; the white patch at the center denotes the flare location. The superimposed contours show the magnetogram, with yellow the positive and blue the negative field.

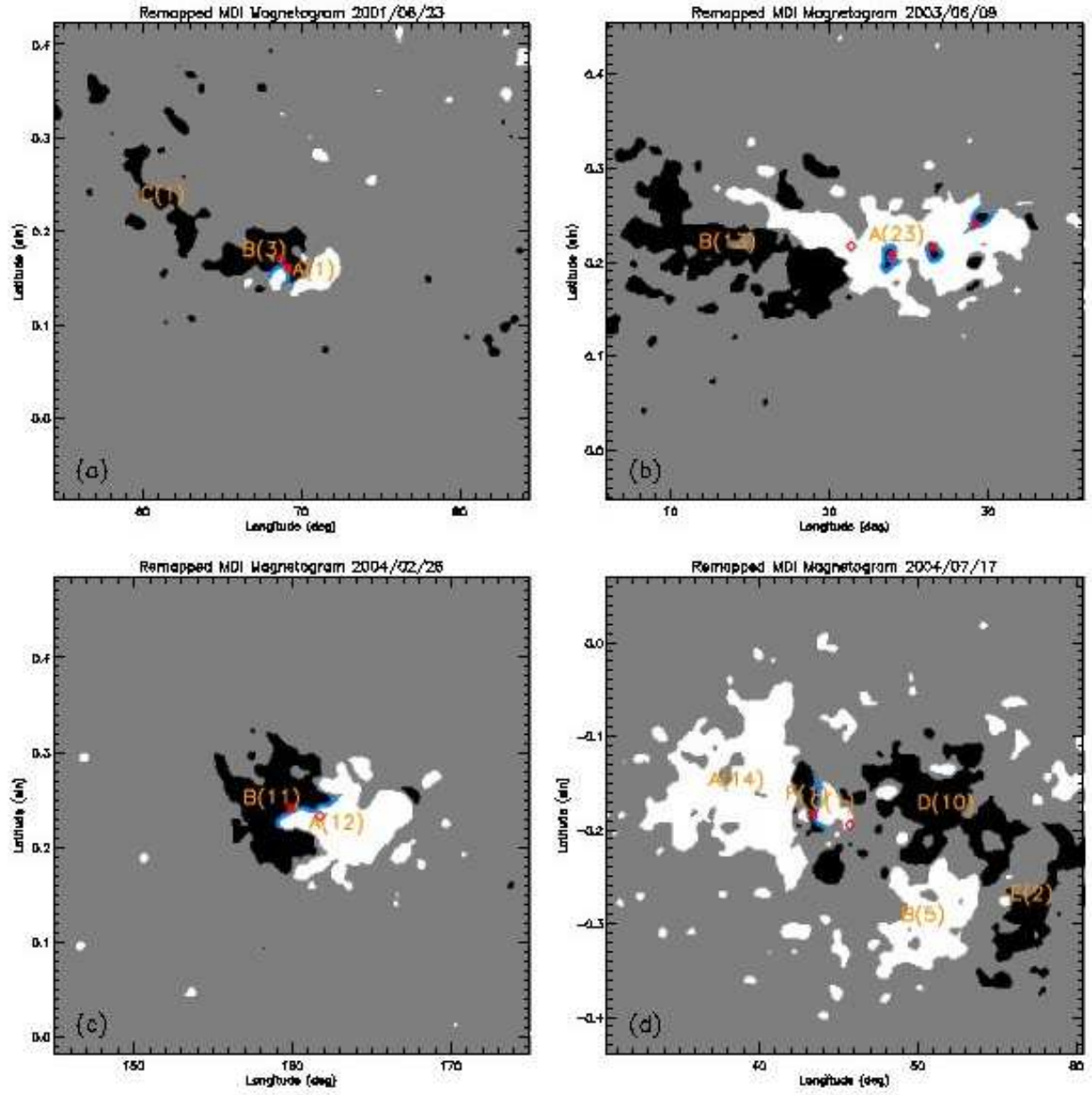

Fig. 3.— Segmented MDI magnetograms for the four confined events, in which strong positive (≥ 50 Gauss) and negative (≤ -50 Gauss) magnetic fields are highlighted as white and black colors, respectively. Red asterisk symbols indicate the flare sites, the red diamond symbols indicate the COM of the active regions, and the blue lines denote the neutral lines over which the flares occurred. See text for more details.

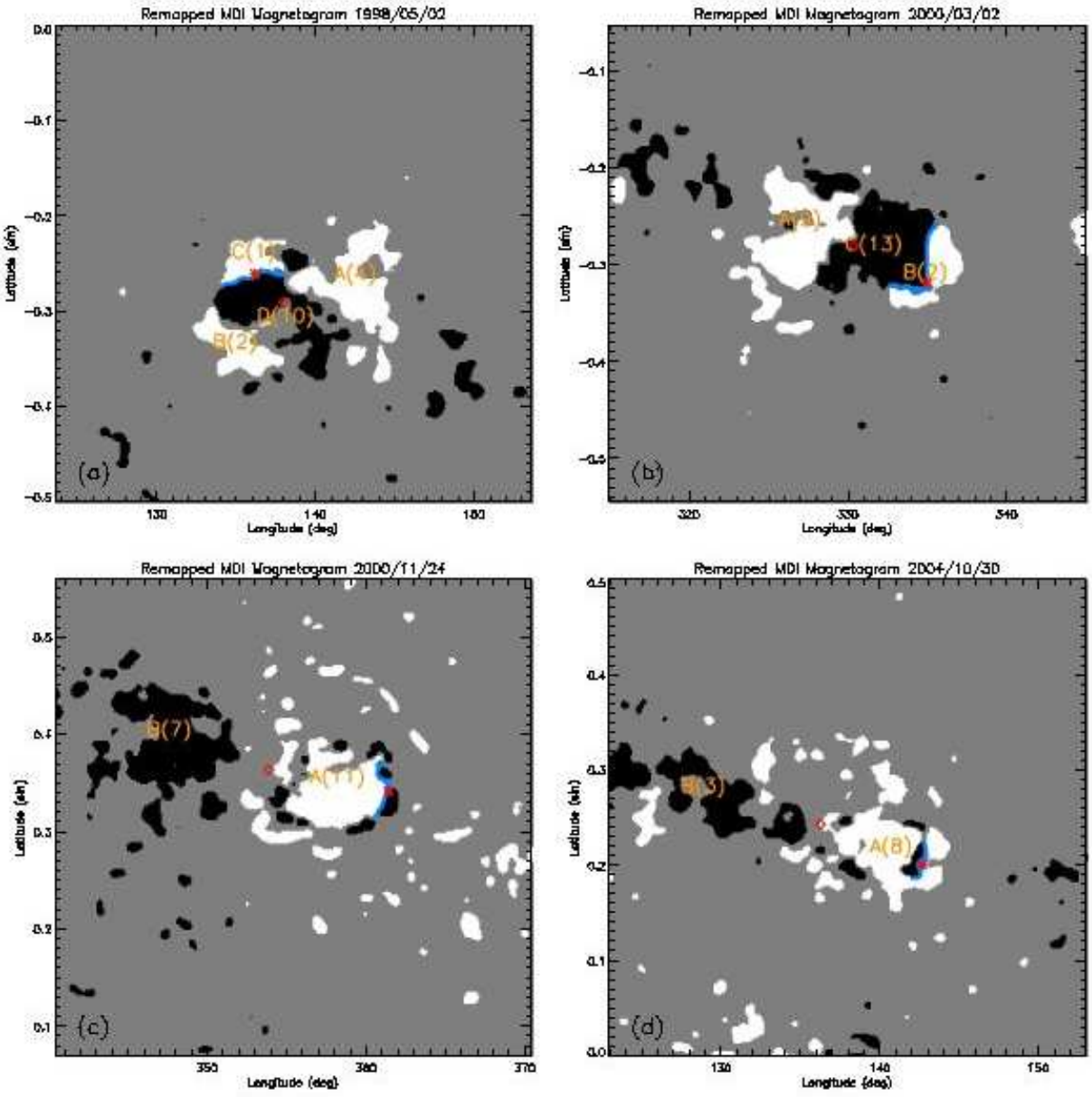

Fig. 4.— Segmented MDI magnetograms for the four eruptive events. See the caption in Figure 3.

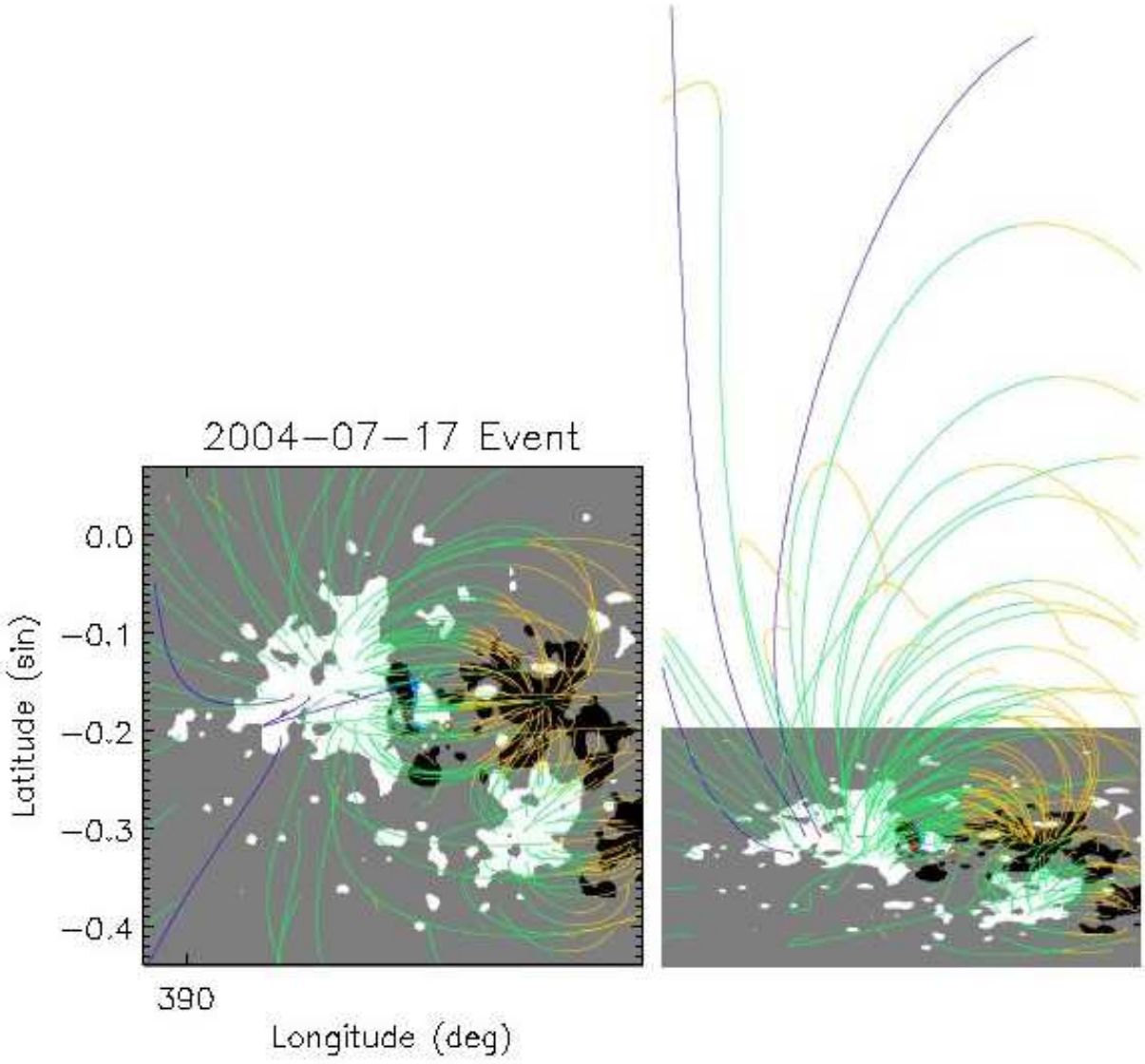

Fig. 5.— Calculated coronal magnetic field of one confined event. The closed field lines are denoted by the green & yellow colors, corresponding to the outward and inward direction respectively, and the open field lines are denoted by the blue color. The left image is of a top view while the right image is of a side view.

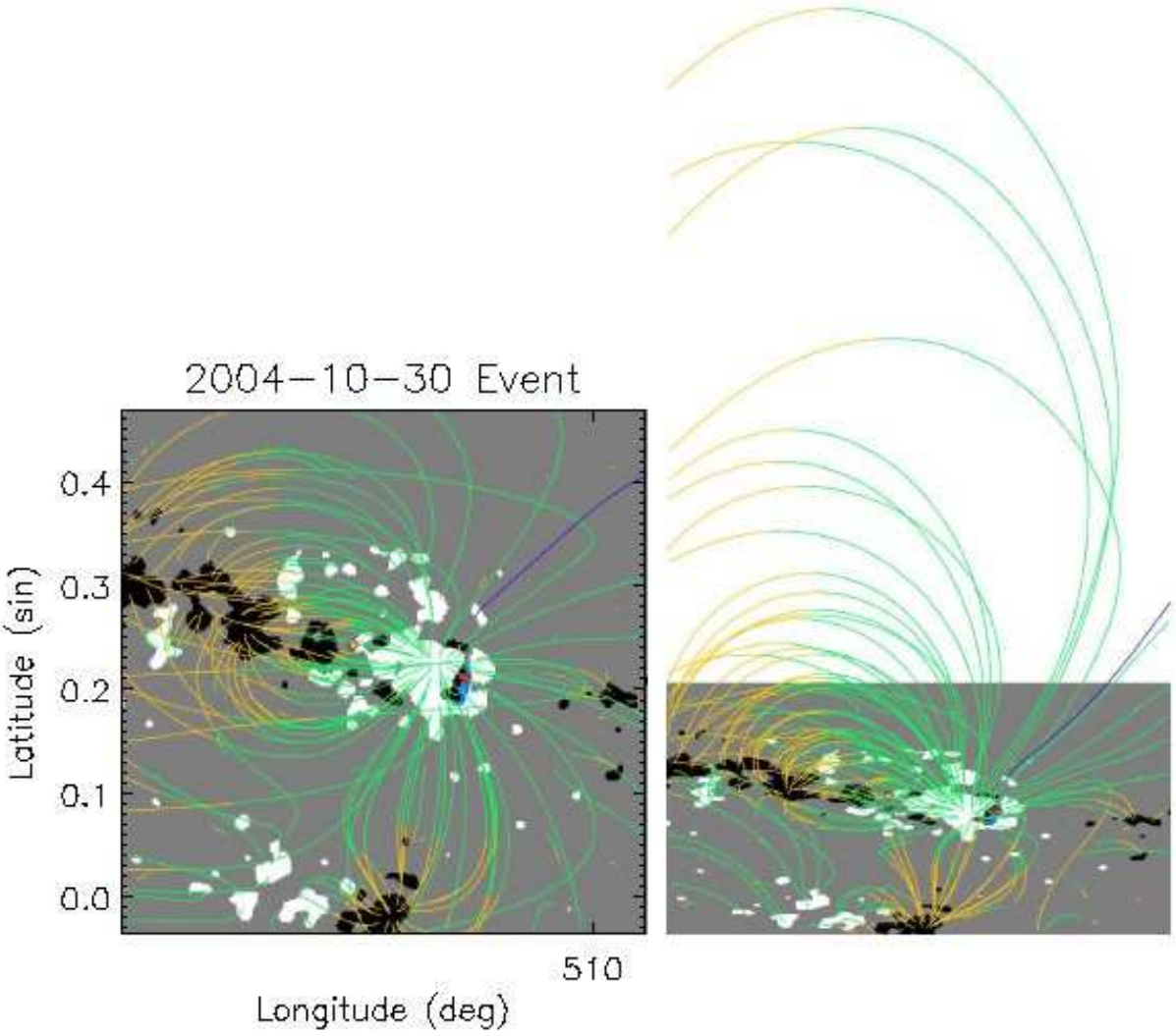

Fig. 6.— An example of eruptive events showing the extrapolated magnetic field above the active region.

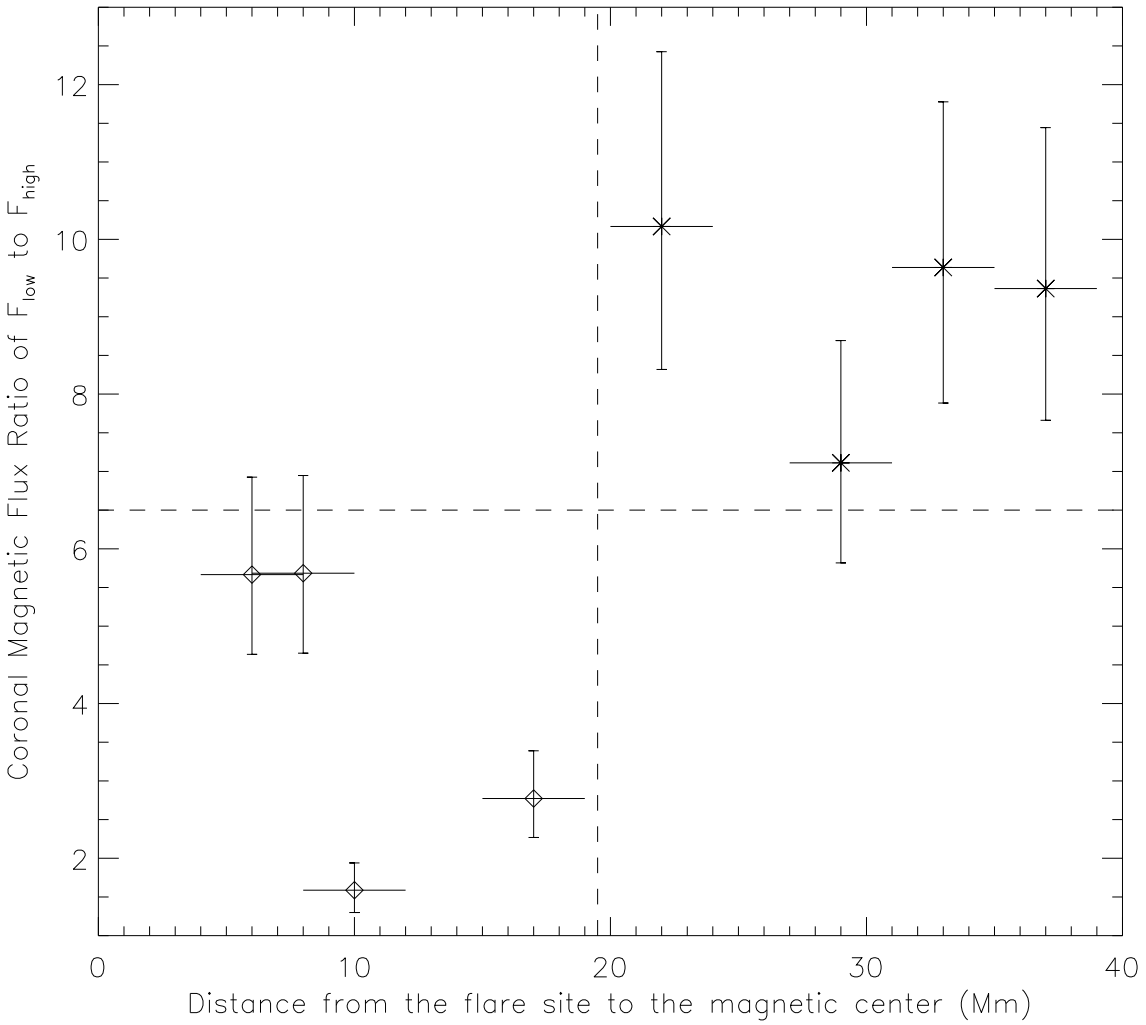

Fig. 7.— The scattering plot showing magnetic properties of both confined events (diamond symbols) and the eruptive events (asterisk symbols). The x-axis denotes the distance between the flare site and the center of magnetic flux distribution (COM) of the active region, and the y-axis denotes the ratio of magnetic flux in the low to high corona above the neutral line.